Efficient Current Injection Into Single Quantum Dots Through Oxide-Confined p-n-Diodes

Markus Kantner, Uwe Bandelow, Thomas Koprucki, Jan-Hindrik Schulze, André Strittmatter, and Hans-Jürgen Wünsche

***Abstract*— Current injection into single quantum dots embedded in vertical p-n-diodes featuring oxide apertures is analyzed in the low-injection regime suitable for single-photon emitters. The experimental and theoretical evidence is found for a rapid lateral spreading of the carriers after passing the oxide aperture in the conventional p-i-n-design. By an alternative design employing p-doping up to the oxide aperture, the current spreading can be suppressed resulting in an enhanced current confinement and increased injection efficiencies, both, in the continuous wave and under pulsed excitation.**

***Index Terms*— Quantum dots (QDs), semiconductor device simulation, single-photon sources (SPSs).**

I. Introduction

EFFICIENT electrical pumping of submicrometer sized domains is essential to achieve deterministic control over the carrier population within nanostructures, such as quantum dots (QDs). This is very important for the generation of single and entangled photons on-demand which is of high interest in the field of quantum optics, quantum information processing, and quantum cryptography [1], [2]. Laterally, oxidized apertures (OAs) are widely implemented into GaAs/AlGaAs-based vertical cavity surface emitting lasers (VCSELs) to provide lateral current as well as optical confinement [3]. The insulating nature of the oxide leads to a funneling of charge carriers into the aperture within the oxide. Moreover, OAs modify the strain field and act as a stressor, which has been successfully used to nucleate single QDs above such apertures deterministically [4], [5]. In combination with the current confinement supplied by the aperture, a very efficient current injection scheme into single QDs can be expected. However, at low-injection levels, our experimental and theoretical data reveal a minor effect of the aperture on the lateral current distribution. In a conventional p-i-n-device layout, the carrier distribution laterally exceeds the dimension of the OA by several micrometers. Our analysis motivates a revised p-n-junction design providing carrier confinement of the order of the aperture size at low-injection levels. To fully understand the mechanisms that prevent efficient current funneling, we simulated several alternative device designs with WIAS-TeSCA [6]. An improved design will be discussed in detail for both continuous wave (CW) and pulsed excitation.

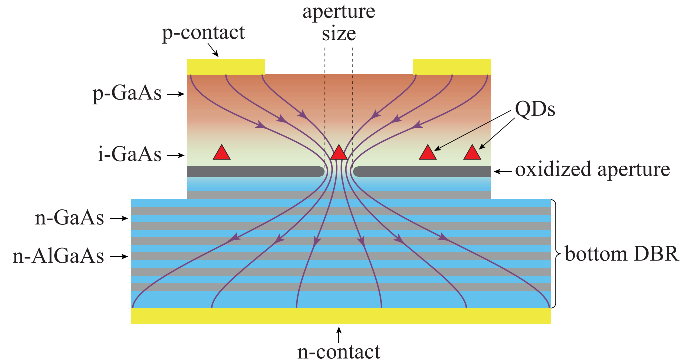

Fig. 1. Schematic cross section of the device. The OA controls the QD nucleation and the current confinement. Triangles: QD positions. Purple lines: intuitive current flow.

II. Experiment

The basic design of a p-i-n-diode featuring an OA is schematically shown in Fig. 1. By applying a two-step epitaxial process, QDs can grow self-aligned at the mesa center due to the strain field of the OA. Using a procedure as detailed below, electrically driven single-photon sources (SPSs) have been demonstrated recently. First, a 24-fold n-doped AlGaAs/GaAs distributed Bragg reflector (DBR) is grown followed by an AlAs/AlGaAs sandwich structure which later forms the OA. The DBR structure is intended to enhance the optical output through the surface of the device. Afterward, mesa structures are processed to expose the aperture layers and allow for wet chemical oxidation. Thereby, an OA is formed acting as a buried stressor, which laterally modifies the strain field at the surface [7]. The QDs are subsequently grown as part of the second epitaxy in the Stranski–Krastanov (SK) growth mode. The growth ends with a p-doped contact layer.

Manuscript received October 9, 2015; revised February 4, 2016; accepted February 25, 2016. Date of publication March 22, 2016; date of current version April 20, 2016. This work was supported by the Deutsche Forschungsgemeinschaft in the framework of the Collaborative Research Center 787 “Semiconductor Nanophotonics” under grants A2 and B4. The review of this paper was arranged by Editor J. Knoch. *(Corresponding author: Markus Kantner.)*

M. Kantner, U. Bandelow, and T. Koprucki are with the Weierstrass Institute for Applied Analysis and Stochastics, 10117 Berlin, Germany (e-mail: kantner@wias-berlin.de; bandelow@wias-berlin.de; koprucki@wias-berlin.de).

J.-H. Schulze and A. Strittmatter are with the Institute of Solid State Physics, Technical University of Berlin, 10623 Berlin, Germany (e-mail: j.schulze@tu-berlin.de; strittma@sol.physik.tu-berlin.de).

H.-J. Wünsche is with the Weierstrass Institute for Applied Analysis and Stochastics, 10117 Berlin, Germany, also with the Ferdinand-Braun-Institut, Leibniz-Institut für Höchstfrequenztechnik, 12489 Berlin, Germany, and also with the Department of Physics, Humboldt University of Berlin, 12489 Berlin, Germany (e-mail: wuensche@wias-berlin.de).

Color versions of one or more of the figures in this paper are available online at http://ieeexplore.ieee.org.

Digital Object Identifier 10.1109/TED.2016.2538561

This work is licensed under a Creative Commons Attribution 3.0 License. For more information, see http://creativecommons.org/licenses/by/3.0/

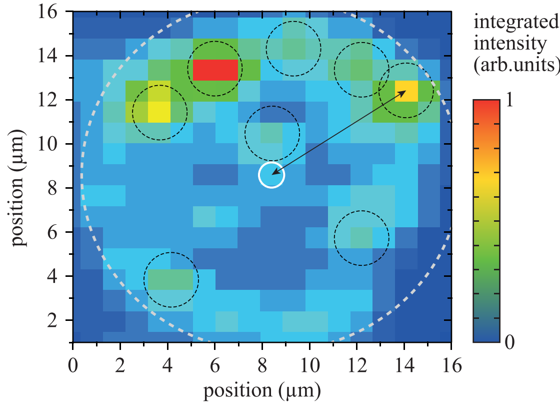

Fig. 2. Electroluminescence map of a mesa at 10 nA with several parasitic QDs recorded at a lateral resolution of 1 μm. The white circle denotes the OA and the arrow corresponds to a distance of 6.7 μm between a parasitic QD and the OA. The figure shows a device where the emission intensity of central QDs is a factor of 30 weaker than from other parasitic QDs. The dashed black circles are a guide to the eye to highlight the positions of parasitic QDs.

Formation of SK-QDs is strain driven where a 2-D to 3-D growth transition occurs at a certain critical layer thickness of about 1.7 monolayers for $In_{0.65}Ga_{0.35}As$/GaAs [8]. Due to the lateral strain variation caused by the OA, the QDs nucleate preferably at positions where the GaAs growth surface is tensely strained. For small aperture diameters, a single tensile strain maximum is formed directly above the aperture. Thus, it is possible to grow site-controlled QDs directly in the center of the mesa with a high selectivity to its surroundings [9]. Highly selective QD nucleation above the OA center is obtained for deposition amounts very close to the critical layer thickness for the 2-D–3-D transition. Fluctuations of the deposition amount across the lateral extension of the p-n-junction region can hardly be avoided and therefore, randomly occurring parasitic QD nucleation must be considered.

An electroluminescence map recorded at a lateral resolution of 1 μm of a 16 μm diameter p-n-diode is shown in Fig. 2. The spectrum recorded directly above the OA (not shown) reveals weak luminescence of about 2–4 QDs. The intensity in the center is a factor of 30 weaker than that originating from the high intensity spots in the outer part of the mesa caused by parasitic QDs. Therefore, this measurement clearly indicates an inhomogeneous excitation of the QDs and insufficient current confinement by the oxide aperture. While the aperture diameter of this particular device is around 800 nm, even QDs located about 7 μm away from the mesa center can be electrically excited. This observation is a contradiction to the naive expectation of the current paths, as shown in Fig. 1. Apparently, the current confinement due to the OA is weak. From the scaling of the device resistance with the diameter of the OA, an insulating property of the oxide is concluded. Consequently, a rapid lateral current spreading after the aperture causing parasitic QD excitation has to be considered.

We use numerical simulations of the charge carrier transport to understand the lateral current spreading after the OA in detail. The simulations are particularly aimed at low-injection currents and cryogenic temperatures as the typical operation conditions of electrically driven SPS.

III. The Model of Current Flow

The excitation of QDs across the whole mesa region is counterintuitive since the radius of the mesa is much larger than the aperture radius and also exceeds typical charge carrier diffusion lengths. Consequently, the carriers injected through the aperture should not be able to reach the parasitic QDs. The experimental finding described above contradicts this expectation.

In order to fully understand this phenomenon, we have performed model calculations. There exists a large number of QD models that treat particles bound to discrete QD states embedded in a macroscopic reservoir of particles in continuum states on different levels of approximation (see recent reviews [10], [11]). However, only a few recent publications include transport in the reservoir [12]–[14] all for macroscopic ensembles of QDs. We are pursuing different approaches, performing fully 3-D current calculations without QDs and treating the impact of single isolated QDs perturbationally. This approach is justified, since the few tiny QDs in our structure have only a weak influence on the transport on large scales. The recombination in a single-shell QD is limited to one electron-hole-pair per lifetime $\tau_{\text{rad}} \approx 1$ ns, which corresponds to a current of about 0.1 nA. This represents a small perturbation of the total current through the device, which is many orders of magnitude larger. This point of view will be detailed and confirmed by control calculations in Section V.

In the framework of the simulation tool WIAS-TeSCA [6], the drift–diffusion transport of unbound carriers is described by the van Roosbroeck system of equations [15], which is a coupled system of Poisson's equation

$$-\nabla \cdot \varepsilon_0 \varepsilon_r \nabla \psi = e \left(p - n + N_D^+ - N_A^- \right) \tag{1}$$

and a continuity equation for each carrier species

$$\begin{aligned} e \frac{\partial p}{\partial t} + \nabla \cdot \mathbf{j}_p &= -eR, \\ -e \frac{\partial n}{\partial t} + \nabla \cdot \mathbf{j}_n &= +eR. \end{aligned} \tag{2}$$

Here, ψ is the electrostatic potential, n and p denote the densities of unbound electrons and holes, respectively, e is the elementary charge, ε_r is the dielectric constant of the semiconductor, ε_0 is the vacuum permittivity, and R combines various recombination mechanisms (Shockley–Read–Hall recombination, Auger recombination, and radiative recombination). The ionized donor and acceptor densities are labeled by N_D^+ and N_A^-. The current densities $\mathbf{j}_n$ and $\mathbf{j}_p$ are modeled in a standard way as drift and diffusion currents [16]. Details and parameters are given in the Appendix.

Two cylindrical mesa designs are compared, which differ only in their doping profile (Fig. 3). The p-i-n-design with layer thickness and doping parameters close to the experimental structure is investigated first. The intrinsic layer will be denoted by cavity (even though it is not an optical cavity) and the embedded QD-layer located 135 nm above the oxide is called active zone (AZ). This particular distance is determined by the optical device design in order to maximize the coupling of the QD-layer to the optical mode. Some details of the

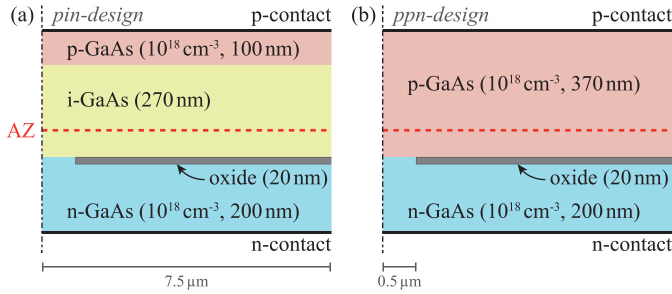

Fig. 3. Sketches of the essential cross sections of the two simulated axissymmetric device structures. (a) p-i-n-design contains a 270-nm-thick intrinsic layer between the n- and p-doped regions. (b) In the p-p-n-design, this layer is also p-doped. The dashed red line labeled AZ is the position of the QD-layer. The QDs are disregarded in the macroscopic transport calculations (see text). The thickness of the current-blocking oxide on top of the n-layer is set to 20 nm. The diameter of the aperture in the center is 1 μm. Except for the oxide, the material is GaAs throughout.

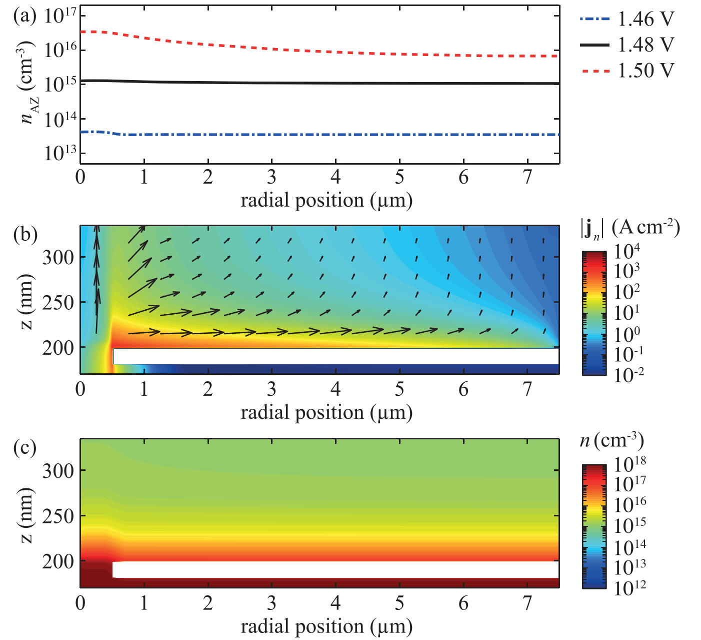

Fig. 4. Analysis of the p-i-n-design. (a) Radial profile of the carrier distributions within the AZ for selected CW bias voltages. Electron and hole densities are identical since the AZ lies in the middle of the intrinsic layer. (b) Electron flow (arrows) and magnitude (color coded) between oxide (white) and AZ (top border) at $U = 1.48$ V. (c) Electron density in the same cross section.

experimental structure (see Fig. 1) have marginal influence on the current distribution between the aperture and the AZ and are, therefore, simplified in the model. The highly conducting cap layer is modeled just as an ohmic contact, neglecting the minimal potential drop across the layer. The same is done to model the complete bottom DBR. Thereby, the interesting current flow between the aperture and the AZ is decoupled from the complex phenomena in the top and bottom layers of the device. For the same reason, the detailed multilayer aperture region of real devices is reduced to a single current-blocking insulator in GaAs with a hole diameter of 1 μm and a thickness of 20 nm. In the simulations, the device temperature is set to $T = 30$ K throughout the paper. It is worth to note here that device simulation at cryogenic temperatures is challenging for the modeling, as well as for the numerics [17], as will be pointed out in the Appendix.

IV. Analysis of Low-Injection CW Operation in the p-i-n-Design

Under CW operation, the carrier density in the AZ increases rapidly with the bias voltage U, in particular in the cryogenic situation. This is shown in Fig. 4(a). In addition, the radial distribution changes when moving from the low-injection to the high-injection case. The density is nearly constant in case of low-injection and starts to drop outward for higher injections.

In this regime, the density in Fig. 4(a) is roughly independent of the radial position in the AZ. Since the capture rate is assumed to be proportional to the density, filling of a QD is expected to be independent on the radial position. This assumption agrees well with the large excitation probability of parasitic QDs described in Section II.

The internal physics behind is also shown in Fig. 4. The electrons flow around the aperture [Fig. 4(b)] and outward in a thin layer on the top of the oxide, where the electron density reaches nearly 10^{18} cm^{-3} [Fig. 4(c) (dark red region)]. This well-conducting layer is radially homogeneous and acts like an equipotential plane. As a consequence, the electron distribution everywhere above it, and, in particular, the injection into the AZ also becomes almost homogeneous along the radial direction.

At the first glance, the high electron mobility might be responsible for the electrons to spread so rapidly. Therefore, it should be beneficial to inject holes through the aperture, whose mobility is much smaller. We accounted for this consideration by exchanging n- and p-doping, but the simulations of a corresponding n-i-p-design yielded nearly no improvement. The holes spread radially along the mesa as well, irrespective of their short diffusion length. We concluded that the mobility is secondary for the extreme spreading in the low-injection regime. Returning to the analysis of the p-i-n-sample, we found a more important factor of influence. Within the intrinsic layer above the oxide, the density of the holes is many orders of magnitude smaller than the electron density. This fact renders that the recombination rate R becomes extremely small. At low temperatures and when other recombination pathways are not limiting, the electron lifetime $\tau_n = n/R$ becomes necessarily extremely long. The simulations yield τ_n up to milliseconds. With such lifetimes, the diffusion length exceeds the mesa radius by many orders of magnitude and the electrons can easily fill the whole mesa area.

Motivated by the importance of this situation, we stress that it is not the matter of the corresponding specific doping configuration, but a general feature of any design containing an intrinsic layer of sufficient thickness under low injection. The space charge zone extends over nearly the whole intrinsic layer. Close to its n-side, it holds $p \ll n$. Furthermore, the Shockley–Read–Hall recombination is the dominant recombination process and an elementary calculation yields the

effective lifetimes

$$\tau_p = \tau_{p,0} \quad \text{and} \quad \tau_n = \frac{n}{p}\tau_{p,0} \gg \tau_p.$$

Mutatis mutandis, this is also valid for the p-side border of the intrinsic layer. The lifetime of the majority exceeds that of the minority by several orders of magnitude. We conclude that the unwanted giant excitation spreading in the low-injection regime is an unavoidable consequence of the cavity being undoped. On the other hand, for devices, such as LEDs and VCSELs, operating under high-injection where diffusion is dominant, the effect of lateral current spreading is minor.

V. Impact of QDs on Free-Carrier Densities

It is generally difficult to model the QD-layer, which is expected to have a randomly fluctuating, discontinuous structure with embedded QDs. We consider first the ideal case, where it contains only the central InAs-QD embedded in the GaAs matrix. The impact of the QD on the current flow can be treated by supplementing the right-hand sides of (1) and (2) by the charge density of bound carriers and capture-escape rates of the QDs, respectively [14]. We assume that the capture-escape processes take place only in a small volume V_{QD} where the free particles overlap with the bound states of the QD. The corresponding capture rate for electrons is modeled as

$$C_n(\mathbf{r}) = \frac{n(\mathbf{r})}{\tau_{n,\mathrm{cap}}}(1 - f_n), \qquad \mathbf{r} \in V_{\mathrm{QD}} \tag{3}$$

within this volume and zero outside. The factor $(1 - f_n)$ accounts for Pauli blocking due to filling of the QD level, $n(\mathbf{r})$ is the bulk carrier density at the QD, and $\tau_{n,\mathrm{cap}}$ is the characteristic capture time of the individual QD. The expression for holes is analogous and the generalization to multiple QDs is straightforward. The escape rates are negligible at low temperatures.

A reasonable value for the capture time can be determined from Dawson *et al.* [18], who have modeled and measured the capture of carriers by a layer of InAs-QDs in a GaAs matrix under excitation of the GaAs. From their photoluminescence measurements, the authors conclude a mean capture rate per volume $\langle C_n \rangle = \gamma_n n$ of the empty QDs with the characteristic (ensemble) capture coefficient $\gamma_n \approx 10^{10}\ \mathrm{s}^{-1}$. The total capture rate per QD is obtained when relating the capture coefficient with the volume filling factor $F = N_D V_{\mathrm{QD}}/h$ of the QDs within the QD-layer. Taking the sheet density of QDs $N_D \approx 10^{10}\ \mathrm{cm}^{-2}$ given in [18], $h \approx 10$ nm for its height, and $V_{\mathrm{QD}} \approx (10\ \mathrm{nm})^3$, this yields a filling factor of $F = 10^{-2}$ and the order-of-magnitude estimates $\tau_{n,\mathrm{cap}} = F/\gamma_n \approx 1$ ps. This estimate for the capture time τ_n agrees well with previously reported capture times in the literature [19]–[21] and is about three orders of magnitude smaller than the typical radiative lifetime $\tau_{\mathrm{rad}} \approx 1$ ns.

The capture rate (3) integrated over the whole QD represents the pump rate for the internal kinetics between the bound states. Under stationary conditions, the pump must balance the losses in time-average. Most prominent loss is the radiative recombination with time-averaged rate $\overline{f_n f_p}/\tau_{\mathrm{rad}}$, which is limited by the recombination rate $1/\tau_{\mathrm{rad}}$ of the filled QD states. At large bulk densities, at the latest when the capture rates of the empty QD exceed the recombination limit, they are kept below the limit by saturation, i.e., the occupations approach unity. The saturation density n_s at which this process starts can be roughly estimated by equating the capture rate of the empty QD with the limit of the radiative rate. This yields $n_s = V_{\mathrm{QD}}^{-1}\tau_{n,\mathrm{cap}}/\tau_{\mathrm{rad}} \approx 10^{15}\ \mathrm{cm}^{-3}$. When raising the bulk densities above n_s, the recombination saturates in the QD but continues growing in the rest of the device, which lowers the quantum efficiency. On the other hand, smaller densities diminish the number of generated photons, which is also unfavorable. Therefore, $n \approx n_s$ represents a certain optimum, which we have chosen for our exemplary calculations.

Let us finally quantify the impact of the capture rate (3) on the macroscopic density distributions. In the worst case $f_n = 0$ (QD is always empty), it acts like an additional recombination within the volume V_{QD} of the QD with an extremely small recombination lifetime $\tau_{n,\mathrm{cap}} \approx 1$ ps. This represents a huge rate and strong spatial hole burning could be expected. However, diffusion spreads this hole to the order of the diffusion length L_D, which exceeds the size of the QD by more than two orders of magnitude. As a consequence, the bulk carrier density is only slightly affected compared with the calculation without capture. We have checked these considerations by the following quantitative control calculations. We repeated the QD-free calculations with setting the lifetime down to 1 ps in a cylindrical QD domain of radius 6 nm and height 10 nm. This yields a reduction of the carrier density by less than one per mille but only in close proximity ($<1\ \mu$m) to QDs. The same also holds for all configurations considered further on in this paper. Therefore, the specific dynamics of carrier capture into up to hundreds of QDs within the mesa are certainly negligible for the purpose of calculating the lateral current and particle distributions in the different devices.

VI. CW Current Confinement in a p-p-n-Design

Considering the findings of Section IV, doping of the cavity region will likely be helpful to suppress the current spreading. The simulation results presented in Fig. 5 for a corresponding p-p-n-design confirm this expectation. The electron lifetime becomes small [Fig. 5(a)] and the current spreading is drastically reduced [Fig. 5(b)]. Accordingly, the radial electron concentration in the AZ decreases rapidly with r, suppressing the excitation of parasitic QDs [see Fig. 5(a)].

Due to the p-doping above the oxide, the injected electrons become minorities and the electron flow is dominated by diffusion. Interestingly, the diffusion length corresponding to the reduced lifetime is still much larger than the radial decrease of $n_{\mathrm{AZ}}(r)$. The additional confinement is related to the vicinity of the p-contact. A considerable part of the injected electrons recombines at the contact, further reducing the mean lifetime. The contact-induced lifetime can be estimated as $\tau_{\mathrm{contact}} \approx d^2/2D$, where d is the distance between the oxide and the contact and $D = k_B T \mu/e$ is the diffusion coefficient. Our parameters yield $\tau_{\mathrm{contact}} \approx 40$ ps, which is nearly three orders of magnitude below the bulk τ_n in Fig. 5(a) and explains the steep decrease of $n_{\mathrm{AZ}}(r)$.

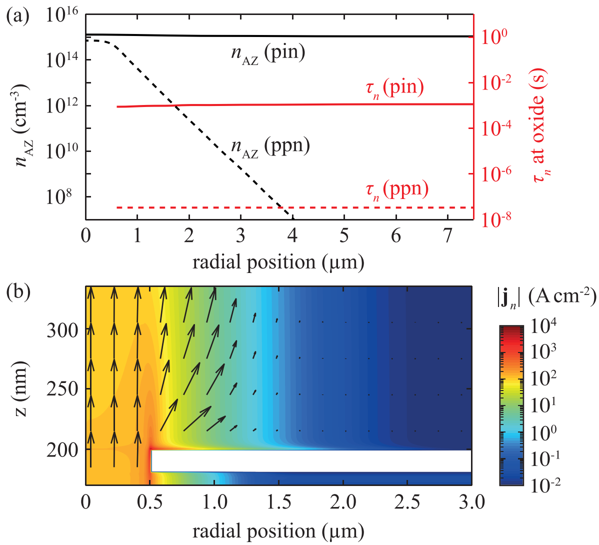

Fig. 5. (a) Radial distributions of the electron density $n_{\mathrm{AZ}}(r)$ in the AZ (black) and the electron lifetime τ_n just above the oxide (red). Solid lines are for the p-i-n-design and dashed lines for the p-p-n-design where the cavity is p-doped with $N_A = 10^{18}$ cm^{-3}. The maximal electron density in the AZ is near $n_{\mathrm{AZ}}(0) = 10^{15}$ cm^{-3} in both cases. (b) Electron current density distribution in the central region between the oxide (white) and the AZ (top border) in the p-p-n-design. Arrows indicate the direction of electron flow and the magnitude is color coded. Note the different radial scale compared with Fig. 4.

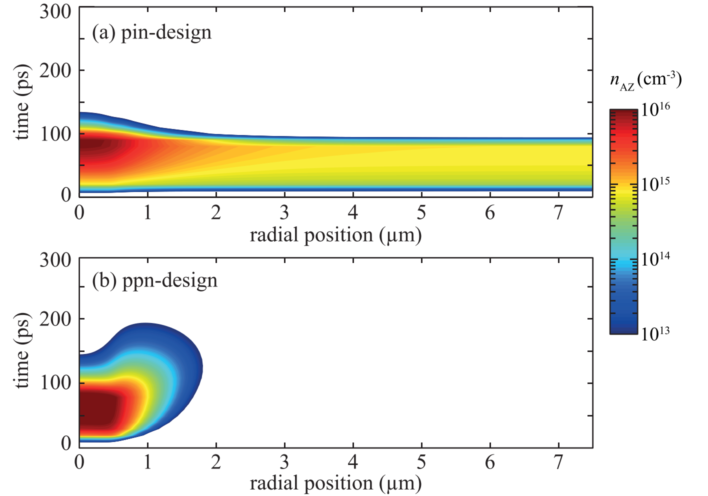

Fig. 6. Response of the electron density in the AZ to a periodically pulsed contact voltage (see text for details). (a) p-i-n-design ($U_0 = 1.43$ V, $\Delta U = 70$ mV). (b) p-p-n-design ($U_0 = 1.48$ V, $\Delta U = 30$ mV). Time is measured relative to the onset of the respective bias pulse. White areas: very small electron densities lower than 10^{13} cm^{-3}.

Concluding so far, the radially homogeneous excitation of the AZ across the whole mesa area is the consequence of keeping the cavity undoped in the standard p-i-n-design. In contrast, the current can be funneled much more to the central QD by using a p-p-n-design with sufficient cavity doping, e.g., $N_A \approx 10^{18}$ cm^{-3} in combination with a small total thickness of the p-layers. The total current increases by these measures. This increase has to be paid to compensate for the larger total recombination. In our simulations, the current for achieving $n_{\mathrm{AZ}} = 10^{15}$ cm^{-3} doubles approximately. This factor is not much in light of the excellent current funneling in an SPS. As a further consequence of doping the AZ, the emission properties of the QDs will be altered. Due to the p-doping, the emission of positively charged complexes (e.g., trions) will become more likely. In turn, this will decrease the emission from the neutral exciton and bi-exciton. Trion ground state emission of QDs exhibits no fine structure splitting [22], [23], which is advantageous for single-photon generation.

VII. Pulsed Operation

For practical applications of an SPS, the deterministic triggering of each photon emission event is essential [2]. Hence, an SPS will be operated in pulsed excitation mode. Furthermore, high repetition rates of the order of GHz are desirable. This requires accordingly short pump pulses. In this section, we investigate whether the results of current spreading under CW excitation hold for the dynamic case of pulsed operation.

To answer this question, we apply 100 ps long bias pulses with a repetition rate of 1 GHz on the top of a constant bias voltage U_0. The bias voltage is chosen just below the threshold voltage of the p-n-diode, such that the electron density in the AZ is slightly below 10^{12} cm^{-3}. Under these conditions, the capture time of the QD is beyond 1 μs, which suppresses captures between pulses. The pulse height ΔU is chosen, such that the capture time raises to the order of the pulse length. The rise and fall time is 20 ps each.

The evolution of the radial electron distributions is shown in Fig. 6. The responses of both designs follow the bias pulse with a delay of only a few picoseconds. We conclude that the internal electronic processes in the cavity are sufficiently fast for pulsed single-photon emission with high repetition rates. Limitations will come from external effects like parasitic capacitances and inductivity of bond wires. These items are not the subject of this paper.

The radial distribution $n_{\mathrm{AZ}}(r, t)$ differs drastically between the two designs under pulsed operation. In the p-i-n-design, it rises homogeneously until about 10^{15} cm^{-3} is reached. Thereafter, the rise is stopped above the oxide. But it continues to about 10^{16} cm^{-3} above the aperture. Accordingly, the probability to capture an electron during the pulse is about 100% for the central QD but only about 10% in the outer region of the mesa. This represents a noticeable reduction of the capture rate for parasitic QDs compared with CW operation but it is probably not small enough to ensure the pure single-photon emission of the device. The pulse-response of the p-p-n-design is entirely restricted to the central part of the mesa. The diameter of the excitation area, where the capture probability of a QD exceeds 1%, is only about 3 μm. Thus, both under CW and pulsed operation, the p-p-n-design is distinctly better suited for current funneling toward the central QD than the p-i-n-design.

VIII. Conclusion

We have shown that the current confinement by a small aperture in an oxide layer can fail under low current injection as applied for single-photon generation with QD-based SPS.

The unintended current spreading is caused by huge differences of the minority and majority charge carrier lifetimes for the given operating conditions. These differences are a direct consequence of the intrinsic region in a p-i-n-design. Our simulations have shown that the doping of the active region leads to much greater current confinement both for CW and pulsed operation. Under pulsed operation, the lateral current spreading can be reduced down to a diameter of 3 μm for a 1 μm wide aperture.

APPENDIX
MODEL EQUATIONS AND PARAMETERS

The fundamental Poisson- and continuity equations (1) and (2) are supplemented by the following model assumptions for GaAs at $T = 30$ K. The relative dielectric constant is taken as $\varepsilon_r = 12.9$ [24] and the recombination rate is

$$R = \left(np - n_i^2\right)\left(\frac{1}{n\tau_{p,0} + p\tau_{n,0}} + B + C_n n + C_p p\right)$$

with $\tau_{p,0} = 34$ ns, $\tau_{n,0} = 10$ ns, $B = 10^{-8}$ cm^3 s^{-1}, and $C_n = C_p = 10^{-30}$ cm^6 s^{-1}. The current densities, carrier densities, and the electrostatic potential are related by

$$\mathbf{j}_n = \mu_n n \nabla F_n, \quad n = N_c \mathcal{F}\left(\frac{F_n - E_c + e\psi}{k_B T}\right)$$
$$\mathbf{j}_p = \mu_p p \nabla F_p, \quad p = N_v \mathcal{F}\left(\frac{E_v - e\psi - F_p}{k_B T}\right) \qquad (4)$$

with the Fermi-Dirac integral

$$\mathcal{F}(\eta) = \frac{2}{\sqrt{\pi}} \int_0^\infty dy \, \frac{\sqrt{y}}{\exp(y - \eta) + 1}$$

of order 1/2. The charge carrier mobilities are assumed as $(\mu_n, \mu_p) = (10^4, 300)$ cm^2 V^{-1} s^{-1} and $(\mu_n, \mu_p) = (6400, 130)$ cm^2 V^{-1} s^{-1} in the intrinsic and doped material, respectively [25]. The effective band densities at $T = 30$ K are $(N_c, N_v) = (1.25, 30) \times 10^{16}$ cm^{-3} and the bandgap is $E_c - E_v = 1.5$ eV. The Fermi levels (F_n, F_p) are calculated from (1) and (2) after inserting (4).

The boundary conditions at the ohmic contacts are $F_n = F_p = eU_i$ and local charge neutrality, where U_i denotes the external voltage applied to contact i. At the other boundaries, the normal components of $\nabla\psi$, $\mathbf{j}_n$ and $\mathbf{j}_p$ vanish.

In the supposed cryogenic situation, the thermal energy is approximately ten times smaller than at room temperature. The carrier densities scale exponentially with the inverse thermal energy as in (4). Consequently, small differences between the band edge energy and the carriers quasi Fermi energy are exponentially enhanced and result in domains with either a very low (depleted semiconductor) or very high (degenerate semiconductor) carrier density, separated by very narrow boundary layers in the thermal equilibrium. In this case, the carrier densities need to be described by the Fermi–Dirac distribution, the Maxwell–Boltzmann approximation is not valid anymore at cryogenic temperatures. For built-in dopant densities below the critical density of the metal-insulator transition [26], one has to take incomplete ionization effects into account. However, for p-doped GaAs:C, the critical acceptor density is given by $N_A^{\mathrm{crit}} \approx 10^{18}$ cm^{-3} [27], and therefore, we assume $N_A^- \approx N_A$ throughout this paper.

REFERENCES

[1] C. Santori, D. Fattal, and Y. Yamamoto, *Single-Photon Devices and Applications*. Weinheim, Germany: Wiley, 2010.

[2] S. Buckley, K. Rivoire, and J. Vučković, "Engineered quantum dot single-photon sources," *Rep. Prog. Phys.*, vol. 75, no. 12, p. 126503, Nov. 2012.

[3] R. Michalzik, Ed., *VCSELs: Fundamentals, Technology and Applications of Vertical-Cavity Surface-Emitting Lasers* (Springer Series in Optical Sciences). Berlin, Germany: Springer, 2013.

[4] W. Unrau *et al.*, "Electrically driven single photon source based on a site-controlled quantum dot with self-aligned current injection," *Appl. Phys. Lett.*, vol. 101, no. 21, p. 211119, 2012.

[5] A. Strittmatter *et al.*, "Site-controlled quantum dot growth on buried oxide stressor layers," *Phys. Status Solidi A*, vol. 209, no. 12, pp. 2411–2420, Nov. 2012.

[6] H. Gajewski and R. Nürnberg. *WIAS-TeSCA: Two- and Three-Dimensional Semiconductor Analysis Package*, accessed on Mar. 10, 2016. [Online]. Available: http://www.wias-berlin.de/software/tesca/

[7] F. Kießling *et al.*, "Strain field of a buried oxide aperture," *Phys. Rev. B*, vol. 91, no. 7, p. 075306, Feb. 2015.

[8] F. Heinrichsdorff, "MOCVD growth and laser applications of In(Ga)As/GaAs quantum dots," Ph.D. dissertation, Dept. Inst. Solid State Phys., Tech. Univ. Berlin, Berlin, Germany, 1998.

[9] A. Strittmatter *et al.*, "Lateral positioning of InGaAs quantum dots using a buried stressor," *Appl. Phys. Lett.*, vol. 100, no. 9, p. 093111, 2012.

[10] W. W. Chow and F. Jahnke, "On the physics of semiconductor quantum dots for applications in lasers and quantum optics," *Prog. Quantum Electron.*, vol. 37, no. 3, pp. 109–184, May 2013.

[11] R. Ferreira and G. Bastard, *Capture and Relaxation in Self-Assembled Semiconductor Quantum Dots*. San Rafael, CA, USA: Morgan & Claypool Publishers, 2015.

[12] M. Gioannini, A. P. Cédola, N. Di Santo, F. Bertazzi, and F. Cappelluti, "Simulation of quantum dot solar cells including carrier intersubband dynamics and transport," *IEEE J. Photovolt.*, vol. 3, no. 4, pp. 1271–1278, Oct. 2013.

[13] M. Kolarczik, N. Owschimikow, B. Herzog, F. Buchholz, Y. I. Kaptan, and U. Woggon, "Exciton dynamics probe the energy structure of a quantum dot-in-a-well system: The role of Coulomb attraction and dimensionality," *Phys. Rev. B*, vol. 91, no. 23, p. 235310, Jun. 2015.

[14] T. Koprucki, A. Wilms, A. Knorr, and U. Bandelow, "Modeling of quantum dot lasers with microscopic treatment of Coulomb effects," *Opt. Quant. Electron.*, vol. 42, nos. 11–13, pp. 777–783, Jun. 2011.

[15] W. Van Roosbroeck, "Theory of the flow of electrons and holes in germanium and other semiconductors," *Bell Syst. Tech. J.*, vol. 29, no. 4, pp. 560–607, Oct. 1950.

[16] S. L. Chuang, *Physics of Photonic Devices*. New York, NY, USA: Wiley, 2009.

[17] M. Kantner, U. Bandelow, T. Koprucki, and H.-J. Wünsche, "Modeling and numerical simulation of electrically pumped single-photon emitters," in *Proc. NUSOD*, Taipei, Taiwan, Sep. 2015, pp. 151–152.

[18] P. Dawson, O. Rubel, S. D. Baranovskii, K. Pierz, P. Thomas, and E. O. Göbel, "Temperature-dependent optical properties of InAs/GaAs quantum dots: Independent carrier versus exciton relaxation," *Phys. Rev. B*, vol. 72, no. 23, p. 235301, Dec. 2005.

[19] A. Wilms, "Coulomb induced interplay of localized and reservoir carriers in semiconductor quantum dots," Ph.D. dissertation, Dept. Inst. Theoretical Phys., Tech. Univ. Berlin, Berlin, Germany, 2013.

[20] A. Wilms, P. Mathé, F. Schulze, T. Koprucki, A. Knorr, and U. Bandelow, "Influence of the carrier reservoir dimensionality on electron-electron scattering in quantum dot materials," *Phys. Rev. B*, vol. 88, no. 23, p. 235421, Dec. 2013.

[21] T. Switaiski *et al.*, "Carrier dynamics in InAs/GaAs submonolayer stacks coupled to Stranski–Krastanov quantum dots," *Phys. Rev. B*, vol. 88, no. 3, p. 035314, Jul. 2013.

[22] J. G. Tischler, A. S. Bracker, D. Gammon, and D. Park, "Fine structure of trions and excitons in single GaAs quantum dots," *Phys. Rev. B*, vol. 66, no. 8, p. 081310, Aug. 2002.

[23] K. V. Kavokin, "Fine structure of the quantum-dot trion," *Phys. Status Solidi A*, vol. 195, no. 3, pp. 592–595, Feb. 2003.

[24] M. Levinshtein, S. Rumyantsev, and M. Shur, *Handbook Series on Semiconductor Parameters*, vol. 2. Singapore: World Scientific, 1996.

[25] V. Palankovski and R. Quay, "Analysis and simulation of heterostructure devices," in *Computational Microelectronics*. Vienna, Austria: Springer, 2004.

[26] N. F. Mott, "Metal-insulator transition," *Rev. Mod. Phys.*, vol. 40, no. 4, pp. 677–683, Oct. 1968.

[27] A. F. da Silva *et al.*, "Electrical resistivity of acceptor carbon in GaAs," *J. Appl. Phys.*, vol. 95, no. 5, p. 2532, 2004.

Markus Kantner has studied physics at Humboldt University of Berlin with a focus on nonlinear dynamics and received his B.S. and M.S. degrees in 2010 and 2013, respectively. Since 2013, he is a Ph.D. student at Weierstrass Institute for Applied Analysis and Stochastics, Berlin, working on modeling and numerical simulation of optoelectronic semiconductor-based devices within the CRC 787 Semiconductor Nanophotonics.

Uwe Bandelow received the Diploma and Ph.D. degrees in physics and the Habilitation degree in theoretical physics from the Humboldt University of Berlin, Germany, in 1991, 1994, and 2009, respectively.

He has been with the Weierstrass Institute for Applied Analysis and Stochastics, Berlin, since 1996. He is teaching as a Privatdozent at the Humboldt University of Berlin on nonlinear phenomena in photonics.

Thomas Koprucki received the Diploma degree in physics from the University of Paderborn, Germany, in 1996, and the Ph.D. degree in mathematics from the Free University of Berlin, Germany, in 2008.

He has been with the Weierstrass Institute for Applied Analysis and Stochastics, Berlin, since 1997. His research interest has been in the area of optoelectronic device modeling and simulation.

Jan-Hindrik Schulze received the Diploma degree in physics with a focus on magneto-optical photoluminescence from the Technical University of Berlin, Germany, where he is currently pursuing the Ph.D. degree with research on epitaxy, processing, and experimental analysis of arsenide-based single photon sources and laser structures within the CRC 787 Semiconductor Nanophotonics.

André Strittmatter received the Diploma degree in physics, the Dr.rer.nat. degree in natural sciences, and the Habilitation degree in experimental physics from the Technical University of Berlin, Germany, in 1996, 2002, and 2012, respectively.

He joined the Institute of Experimental Physics, University of Magdeburg, Germany, in 2014, as an Interim Head of the Group for Semiconductor Epitaxy, where he is involved in nitride-based devices.

Hans-Jürgen Wünsche, photograph and biography not available at the time of publication.